M. Eugene Rudd Publications   Research Papers in Physics and Astronomy
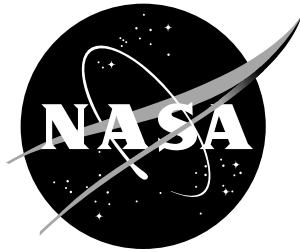
12-1997

Shielding Strategies for Human Space Exploration Chapter 9: HZE Interactions in Biological Materials

M. Eugene Rudd
University of Nebraska - Lincoln, erudd@unl.edu

Shielding Strategies for Human Space Exploration

Edited by
J. W. Wilson, J. Miller, A. Konradi, and F. A. Cucinotta
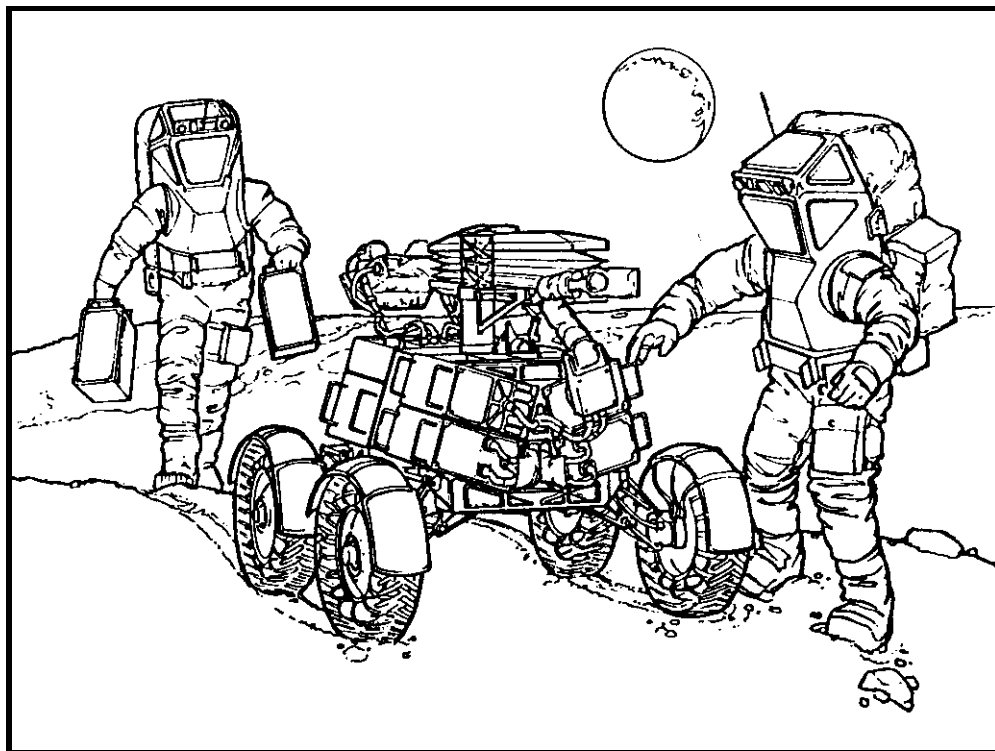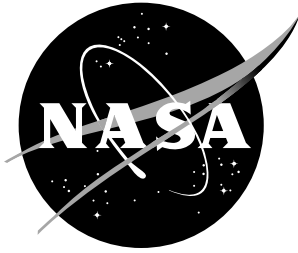
Shielding Strategies for Human Space Exploration

Edited by
J. W. Wilson
Langley Research Center • Hampton, Virginia

J. Miller
Lawrence Berkeley National Laboratory • Berkeley, California

A. Konradi
Lyndon B. Johnson Space Center • Houston, Texas

F. A. Cucinotta
Langley Research Center • Hampton, Virginia

December 1997

CHAPTER 9

HZE INTERACTIONS IN BIOLOGICAL MATERIALS

by

M. Eugene Rudd[1]

[1]Department of Physics and Astronomy, University of Nebraska, Lincoln, Nebraska 68588

Chapter 9

HZE INTERACTIONS IN BIOLOGICAL MATERIALS

SUMMARY

It is shown that most of the energy deposited by fast charged particles traversing matter occurs through ionization, i.e., the ejection of electrons during the atomic collision. The important mechanisms of ionization are identified and several methods of calculating the relevant differential and total cross sections are described. These include both classical and quantum theoretical methods and two semi-empirical models. The calculational methods were intended only for light, bare-ion projectiles, and care must be exercised in extending them to heavy, dressed projectiles.

IMPORTANCE OF IONIZATION

Fast charged particles traversing matter lose energy in successive collisions through three main processes: excitation, charge transfer, and ionization. Since ionization is not only the most probable of the three processes but also the one that involves the largest energy transfer, it is the one that contributes most to the stopping power. Energy must be transferred to overcome the binding energy (or ionization potential) in addition to that which provides the kinetic energy of the ejected electron or electrons. Furthermore, a sizable fraction of the ejected electrons (roughly half) have a high enough energy to cause further ionization. For these reasons, an understanding of radiation effects caused by fast charged particles requires data on ionization. Figure 1 shows the contributions to the stopping power by the three processes for proton impact on water vapor. At high energies, where charge transfer has dropped off to a negligible value, the sum of the fractions due to secondary electron kinetic energy F_ε and overcoming binding F_B account for over 80% of the stopping power with excitation contributing the rest. Thus, to make a comprehensive model of energy deposition, the systematics of electron production must be known.

INFORMATION NEEDED

To model the deposition of energy by charged particle interactions with matter, the following information is required:

1. The angular distributions of secondary electrons are needed to determine the spatial pattern of energy deposition.

2. The energy distributions of secondary electrons are needed to find the energy loss per ionization event, i.e., the stopping power.

3. Total ionization cross sections are required to calculate the mean free paths between ionizing events.

Unfortunately, ionization is a complex process, even for simple incident particles such as electrons and protons and is more complex for heavy, bare-nucleus projectiles. Heavy, dressed projectiles (i.e., those carrying electrons) have additional complications. We begin with a description of light ion (mostly proton) impact ionization because (a) many processes are the same as for heavy ions, and (b) most of the existing data and theories are for light ions, but these can often be extrapolated to apply to heavy ions.

CROSS SECTIONS

To make information on collisions useful we need to know the probabilities for various collision events. The quantitative measure of probability in atomic physics is the cross section which is a measure of how large the target looks to an incoming beam of ions for a given process. The total ionization cross section (or TICS) is measured in area units such as cm^2 or m^2. We also define singly differential cross sections (SDCSs) which are measured in units of area per unit ejected electron energy or area per unit solid angle, and doubly differential cross sections (DDCSs) measured in units of area per unit energy per unit solid angle. By integration, one can calculate the SDCSs and the TICSs from the DDCSs. Measurements of DDCSs are available for protons on many gases from a few keV to several MeV energy and for some heavy ions up to about 1000 MeV.

MECHANISMS OF ELECTRON EMISSION

The process of ionization can take place through one or more of several mechanisms. Some of the most important of these are:

1. Distant, soft collisions produce a peak at zero in the energy spectrum of electrons and an almost isotropic angular distribution.

2. Close, hard collisions are binary or billiard-ball-type interactions with a single electron in the target. Such collisions yield a peak in the spectrum of electrons at a secondary energy related to the angle of ejection through momentum and energy conservation.

3. Autoionization and Auger emission are processes that involve transitions between sharply defined energy levels and therefore yield sharp peaks in the energy spectra. Except in certain spectral regions, these mechanisms do not contribute much to the cross sections.

4. Projectile ionization (electron loss). A dressed ion (or atom) incident on a target may be thought of as a set of loosely bound electrons moving with the projectile which are easily detached, making elastic collisions with the target. While they may come off at any angle, they are found mostly in the forward directions. They produce a broad peak in the spectrum centered at the speed of the projectile.

Figure 2, showing energy spectra at different emission angles for electrons from 30-MeV $O^{5+} + O_2$ collisions, illustrates these mechanisms and their dependence on angle.

THEORETICAL METHODS

Several classical and quantum mechanical methods have been used to calculate electron ejection cross sections. Most of them account only for the soft, distant collision mechanism and the binary collision mechanism. The more elaborate methods generally yield better accuracy than the simple ones and are often more widely applicable. However, we will consider only a few of the simpler, more widely used methods.

Rutherford Equation

The Rutherford equation [1] was derived classically on the assumption that the electron in the target is initially at rest but held by a binding energy B. The total cross section is

$$\sigma_R = \frac{4\pi a_0^2 R^2}{TB} \tag{1}$$

where $T = m_e v^2/2$, m_e is the mass of the electron, v is the velocity of the projectile, a_0 is the Bohr radius (=0.529 Å), and R is the Rydberg of energy (=13.6 eV). The differential form of the equation is

$$\sigma_R(\varepsilon) = \frac{d\sigma}{d\varepsilon} = \frac{4\pi a_0^2 R^2}{TQ^2} \tag{2}$$

with $Q = B + \varepsilon$ where ε is the kinetic energy of the ejected electron. This form of the equation is often used with the kinematic cutoff at $\varepsilon = 4T = 2m_e v^2$.

Binary Encounter Approximation or BEA

The binary encounter approximation (BEA) takes account of the initial orbital motion of the electrons [2], but assumes that all electrons in the same shell have the same energy, U. The SDCS is

$$\sigma(\varepsilon) = \sigma_R(\varepsilon)\left(1 + \frac{4U}{3Q}\right), \qquad B \leq Q \leq Q_- \tag{3}$$

$$\sigma(\varepsilon) = \sigma_R(\varepsilon)\frac{U}{6Q}\left[\left(\frac{4T}{U}\right)^{3/2} + \left(1 - \sqrt{1 + \frac{Q}{U}}\right)^3\right], \qquad Q_- \leq Q \leq Q_+ \tag{4}$$

where $Q_\pm = 4T \pm 4(TU)^{1/2}$.

Binary Encounter Approximation With Fock Distribution

If one assumes a Fock hydrogenic distribution of velocities of the orbital electron and integrates over that distribution, the result is called the BEA-F equation [3]. It is stated in terms of the quantities $\alpha = Q/B$, $\phi = \left(T/\overline{U}\right)^{1/2}$ and $\beta = (\alpha/4\phi - \phi)^2$, where $\overline{U}$ is the average orbital kinetic energy.

$$\sigma(Q) = \sigma_A + \sigma_B, \quad \text{for} \quad B \leq Q \leq 4T \tag{5}$$

$$\sigma(Q) = \sigma_B, \quad \text{for} \quad Q \geq 4T \tag{6}$$

where

$$\sigma_A = \sigma_R(Q)\frac{\overline{U}}{\pi Q}\left[\frac{32\beta^{3/2}\alpha}{3(1+\beta)^3} + (4/3+\alpha)(\pi - 2R_1)\right] \tag{7}$$

$$\sigma_B = \sigma_R(Q)\frac{\overline{U}}{\pi Q}\left[\frac{16}{3(1+\beta)^3}\left(\frac{4\phi^3}{3} - \beta^{3/2}\alpha - \frac{\alpha(\alpha+\beta)^{3/2}}{1-\alpha}\right)\right.$$
$$\left. + \left(\frac{4}{3}+\alpha\right)R_1 - \left(\frac{4}{3} - \frac{\alpha}{1-\alpha}\right)R_2\right] \tag{8}$$

with

$$R_1 = \tan^{-1}\beta^{-1/2} + \frac{\beta^{1/2}}{(1+\beta)^3}\left(1 + \frac{8}{3}\beta - \beta^2\right) \tag{9}$$

and

$$R_2 = R_3 + (1-\alpha)^{-3/2}\tan^{-1}\left(\frac{1-\alpha}{\alpha+\beta}\right)^{1/2}, \quad for \quad \alpha < 1$$
$$= R_3 + (\alpha-1)^{-3/2}\ln\frac{(\alpha+\beta)^{1/2} - (\alpha-1)^{1/2}}{(1+\beta)^{1/2}}, \quad for \quad \alpha > 1 \tag{10}$$

and

$$R_3 = \left(2 + \frac{14}{3}\beta + \frac{8}{3}\alpha\right)\frac{(\alpha+\beta)^{1/2}}{(1+\beta)^3} - \frac{(\alpha+\beta)^{1/2}}{(1+\beta)(1-\alpha)} \tag{11}$$

Although this appears somewhat complicated, it is an analytic equation and can easily be programmed on a desk computer to produce cross sections for any given target, projectile energy, and secondary electron energy. The quantities B and U needed for the computation are given in the literature for a wide range of atomic and molecular targets [4]. In multishell targets the computation on these models is made for each shell, using the proper B and U

values, and then added. Usually only the outermost two or three shells contribute much to the cross section. There is a comparison of the Rutherford, BEA, and BEA-F equations with experimental data in Fig. 3.

Plane-wave Born Approximation

This is a quantum mechanical treatment which has been widely used. It assumes that the incident ion is deflected only slightly in its interaction with an electron in the target and also assumes a hydrogen wave function, scaled by the effective charge. It is generally fairly accurate at high energies (>500 keV/u) for relatively simple targets and projectiles.

$$\sigma(\varepsilon,\theta) = \frac{2^8 m_p^2}{k^2} \int_{q_m}^{q} \max \frac{1}{q} \frac{\mu^6 \exp\left\{-2\mu\big/\kappa \tan^{-1}\left[2\kappa\mu\big/\left(q^2 - \kappa^2 + \mu^2\right)\right]\right\}}{q\left[(q+\kappa)^2 + \mu^2\right]\left[(q-\kappa)^2 + \mu^2\right]\left[1 - \exp(-2\mu/\kappa)\right]}$$
$$\times \frac{CD^3 + 4CDE^2 - 4BD^2E - BE^3 + 2AD^3 + 3ADE^2}{\left(D^2 - E^2\right)} dq, \tag{12}$$

where

$$A = q^2 - 2q_m\kappa\cos\theta + \left(\kappa^2 + \mu^2\right)\left(q_m/q\right)^2 \cos^2\theta$$
$$B = 2\left(q^2 - q_m^2\right)^{1/2}\kappa\sin\theta - \left(\kappa^2 + \mu^2\right)\left(2q_m/q^2\right)\left(q^2 - q_m^2\right)^{1/2}\sin\theta\cos\theta$$
$$C = \left(\kappa^2 + \mu^2\right)\left[\left(q^2 - q_m^2\right)\big/q^2\right]\sin^2\theta \tag{13}$$
$$D = q^2 - 2q_m\kappa\cos\theta + \kappa^2 + \mu^2$$
$$E = 2\kappa\left(q^2 - q_m^2\right)^{1/2}\sin\theta$$

θ is the angle of ejection of the electron, $q_m \approx (m/2)\left(\kappa^2 + \mu^2\right)\big/k$, k is the wave vector for the incident ion in the laboratory system, κ is the wave vector of the ejected electron, $\mu = \left(B/R\right)^{1/2}$, and $q_{\max} \approx 2\kappa$. Cross sections are obtained by doing the integration over q numerically. Figure 4 shows a comparison of measured DDCSs with those calculated on the Born approximation and on the BEA. The agreement is good at intermediate angles but at the lower ejected energies, there are large discrepancies at small and large angles. The Born approximation is better for the large angles than the BEA, but still much too low. Both do poorly at small angles. These faults have been corrected in more sophisticated theoretical treatments.

SEMI-EMPIRICAL ANALYTICAL MODELS

Many users of cross section data are less interested in a rigorously derived theoretical equation than in a simple method of obtaining reasonably accurate cross sections. Many semi-empirical analytical models provide relatively simple equations or methods which yield such cross sections. Most analytical models require either some experimental data as input or values of a number of adjustable parameters. If the parameters have already been

determined from experiment, the model immediately yields the needed cross sections. Two such models will be described.

The Miller Model

The Miller model [5] is based on the Bethe equation which may be written

$$\sigma(\varepsilon) = \frac{4\pi a_0^2 R}{T}\left[\frac{R}{Q}\frac{df}{dQ}\ln\frac{4T}{R} + b(\varepsilon)\right] \tag{14}$$

where $Q = B + \varepsilon$, B is the ionization potential, ε is the ejected electron energy, and df/dQ is the differential optical oscillator strength. Quite accurate values of the latter quantity can be obtained from photoionization measurements. The first term of the Bethe equation is the "soft-collision" term; the second is the "hard-collision" term. Since the quantity $b(\varepsilon)$ is independent of projectile properties, it can be determined by subtracting the first term from one experimental spectrum of $\sigma(\varepsilon)$ at one incident energy. Then $b(\varepsilon)$ can be used for all incident energies. The model is most useful for large projectile energies. Figure 5 shows the good agreement between calculations using the Miller model and experimental energy distributions.

The Rudd Model

The Rudd model [6], which is based on Bethe equation, the BEA, and on molecular promotion theory, is useful at all incident energies and all electron energies. To obtain an electron spectrum at one incident energy, one needs to know 3 parameters, F_1, F_2, and α. To obtain spectra at all incident energies requires 10 parameters. The SDCS is given by

$$\sigma(w) = \frac{S}{B}\frac{F_1 + F_2 w}{(1+w)^3\{1 + \exp[a(w - w_c)/v]\}}$$

where $w = \varepsilon/B, v^2 = T/B, w_c = 4v^2 - 2v - R/4B, S = 4\pi_0^2\, a_o^2 N(R/B)^2$, N is the number of electrons, and where

$$F_1 = L_1 + H_1 \qquad\qquad F_2 = L_2 H_2/(L_2 + H_2)$$
$$L_1 = C_1 v^{D1}/(1 + E_1 v^{D1+4}) \qquad L_2 = C_1 v^{D2}$$
$$H_1 = A_1 \ln(1 + v^2)(v^2 + B_1/v^2) \qquad H_2 = A_2/v^2 + B_2/v^4$$

Values of the ten parameters, $A_1, B_1, ...E_1, A_2, B_2, ...D_2$, and α for many of the simple atomic and molecular gases are given in Table 1.

A sample of the fit of the Rudd model is given in Fig. 6 showing the energy spectra of electrons from $H^+ + H_2O$ collisions at 15–1000 keV. The quantity $Y = \sigma(\varepsilon)/\sigma_R(\varepsilon)$, which is the ratio of the SDCS to the corresponding Rutherford cross section, is plotted instead of the SDCS itself in order to reduce the large range of values and to make a more compact graph. The solid lines represent the model and the circles and crosses are measured values.

HEAVY BARE PROJECTILES

Most theoretical treatments yield collision cross sections which are proportional to Z^2, where Z is the charge of the projectile. This allows easy scaling from proton calculations, e.g., to any heavy bare ion projectile. Unfortunately, there are limitations to Z^2 scaling, especially for very high Z projectiles. There are at least three reasons for this: (1) for a given impact parameter, the probability of an ionization increases for increasing Z, but as the probability approaches unity, saturation limits its increase, (2) multiple ionization, which is an important contribution to the overall ionization cross section for heavy incident ions, does not scale as Z^2, and (3) simple theories do not account for two-center effects, that is, emission of electrons in which the fields of both the residual target ion and the incident ion affect the trajectories of emitted electrons.

The criterion for Z^2 scaling to hold is that $Zv_0/v \ll 1$ where v is the projectile velocity and v_o is the Bohr velocity. The failure of Z^2 scaling is illustrated in Fig. 7, where the total ionization cross sections for heavy bare-ion impact divided by the corresponding proton cross sections and by Z^2 are plotted against the energy per unit mass of the incident ion. The dotted line at unity indicates the results expected if Z^2 scaling held. At low incident velocities and especially for high Z projectiles, the cross sections fall off from the expected values.

A further example of Z^2 scaling failure is shown in Figure 8 for 25-MeV Mo^{40+} ions incident on helium. The energy spectra of electrons emitted at a forward angle, 20°, and a backward angle, 150°, are shown. The cross

Table 1. Parameters for fitting SDCSs to the Rudd Model

	He	Ne	Ar	Kr	H_2	N_2	0_2	H_2O	CO_2	CH_4	Inner Shells
A_1	1.02	0.58	1.20	1.46	0.96	1.05	1.02	0.97	1.09	1.15	1.25
B_1	2.4	65	8.0	5.7	2.6	12.0	50	82	25	14	0.50
C_1	0.70	0.23	0.86	0.65	0.38	0.74	0.40	0.40	0.75	0.35	1.00
D_1	1.15	0.55	0	−0.55	0.23	−0.39	0.12	−0.30	0.75	0.50	1.00
E_1	0.70	0.16	0.80	1.00	2.2	0.80	0.30	0.38	0.65	3.0	3.0
A_2	0.84	1.40	0.90	1.30	1.04	0.95	1.00	1.04	0.78	0.60	1.10
B_2	6.0	0	2.7	22	5.9	1.20	5.0	17.3	3.0	3.8	1.30
C_2	0.70	0.72	0.75	0.95	1.15	1.00	0.55	0.76	0.70	1.20	1.00
D_2	0.50	1.35	0.80	−1.00	0.20	1.30	0	0.04	0.85	0.45	0
α	0.86	0.57	0.71	0.78	0.87	0.70	0.59	0.64	0.53	0.61	0.66

sections have been divided by 1600 times the equal velocity proton cross sections. Thus, if Z^2 scaling held, the result should be unity as shown by the dashed line. However, the high-Z projectile evidently drags some of the electrons initially directed in the backward direction into the forward direction. Such two-center effects are important for electron emission in all directions. Furthermore, they are most important for $v_e \cong v_{ion}$. Also plotted in Fig. 8 are calculations made on the continuum-distorted wave–Eikonal-initial-state (CDW-EIS) theory, a relatively recent quantum mechanical model that takes the effects of both collision centers into account.

HEAVY DRESSED PROJECTILES

There are additional complications if the incident ion carries electrons. Some of these are: (1) The emission of projectile electrons. This was already discussed briefly earlier. (2) The possibility of simultaneous excitation and ionization. This provides an additional channel for the emission of electrons and in any calculation of cross sections it must be taken into account. An example is given in Fig. 9 showing the angular distributions of 218-eV electrons from 0.5-MeV/u He^+ + He collisions. In the calculation four reactions are combined to approximate the experimental distribution. The four are: (a) projectile ionization with the target remaining in the ground state, (b) projectile ionization with simultaneous target excitation, (c) target ionization with the projectile remaining in the ground state, and (d) target ionization with simultaneous projectile ionization. Note that all four contribute substantially to the total. (3) Screening effects. The nuclear charge of a dressed projectile is partially screened by the electrons it carries. When a projectile of nuclear charge Z carrying N electrons passes a target at a large distance, it looks to the target like an ion of charge Z-N. However, if it makes a very close collision the full charge Z is effective. This difference of screening has to be considered in calculating cross sections for dressed-ion collisions. An example of the effect of this change in screening is shown in Fig. 10 which compares the energy spectra of electrons for 0.5-MeV/u H^+, He^+, and He^{2+} ions incident on helium atoms. Consider the He^+ curve. The low energy ejected electrons come primarily from distant collisions for which the projectile's electron provides almost complete screening, making the projectile look like a proton. The high energy electrons, however, come mostly from very close collisions for which the nucleus is not screened and therefore yields a cross section close to that of the He^{2+}.

TWO USEFUL REPORTS

There are two extensive reports, both recently published, which review the subject of electron emission by charged particle interactions with matter. These should be especially useful to those who need cross sections for modelling the interaction of charged particle radiation with matter. One is *Atomic and Molecular Data for Radiotherapy and Radiation Research*, IAEA-TECDOC-799, May 1995, 754 pages. This is obtainable from Nuclear Data Section, International Atomic Energy Agency, Wagramerstrasse 5, P.O. Box 100, A-1400 Vienna, Austria. The other is *Secondary Electron Spectra from Charged Particle Interactions*, ICRU Report 55. This may be obtained from the International Commission on Radiation Units and Measurements, 7910 Woodmont Avenue, Bethesda, MD 20814.

REFERENCES

1. E. Rutherford: The scattering of α and β particles by matter and the structure of the atom. *Phil. Mag.* **21**: 669–688; 1911.

2. L. H. Thomas: The effect of orbital velocity of the electrons in heavy atoms on their stopping of α-particles. *Proc. Cambr. Phil. Soc.* **23**: 713–716; 1927.

3. M. E. Rudd, D. Gregoire, and J. B. Crooks: Comparison of experimental and theoretical values of cross sections for electron production by proton impact. *Phys. Rev.* A **3**: 1635–1640; 1971.

4. M. E. Rudd, Y. -K. Kim, D. H. Madison, and T. J. Gay: Electron production in proton collisions with atoms and molecules: energy distributions. *Rev. Mod. Phys.* **64**: 441–490 and W. Hwang, Y. -K. Kim and M. E. Rudd; New model for electron-impact ionization cross sections of molecules. *J. Chem Phys.* **104**: 2956–2966; 1996.

5. J. H. Miller, L. H. Toburen, and Steven T. Manson: Differential cross sections for ionization of helium, neon, and argon by high-velocity ions. *Phys. Rev.* A **27**: 1337–1344; 1983.

6. M. E. Rudd: Differential cross sections for secondary electron production by proton impact. *Phys. Rev.* A **38**: 6129–6137; 1988.

7. W. E. Wilson: Stopping power partition and mean energy loss for energetic protons in hydrogen. *Radiat. Res.* A **49**: 36–50; 1972.

8. N. Stolterfoht, D. Schneider, D. Burch. H. Wiemann, and J. S. Risley: Mechanisms for electron production in 30-MeV $O^{n+} + O_2$ collisions. *Phys. Rev. Lett.* **33**: 59–62; 1974.

9. M. E. Rudd and J. H. Macek: Mechanisms of electron production in ion-atom collisions. Case Studies in Atomic Physics **3**: No. 2, 47–136; 1972.

10. J. H. Miller, L. H. Toburen, and Steven T. Manson: Differential cross sections for ionization of helium, neon, and argon by high-velocity ions. *Phys. Rev.* A **27**: 1337–1344; 1983.

11. M. E. Rudd, Y. -K. Kim; D. H. Madison, and T. J. Gay: Electron production in proton collisions with atoms and molecules: Energy distributions. *Rev. Mod. Phys.* **64**: 441–490; 1992.

12. P. D. Fainstein, V. H. Ponce, and R. D. Rivarola: Electron emission for multielectronic atoms by ion impact at intermediate and high energies. *J. Phys.* B **20**: 1207–1215; 1991.

13. N. Stolterfoht, D. Schneider, J. Tanis, H. Altevogt, A. Salin, P. D. Fainstein, R. Rivarola, J. P. Grandin, J. N. Scheurer, S. Andriamonje, D. B. Ertault, and J. F. Chemin: *Europhys. Lett.* **4**: 899–904; 1987.

14. S. T. Manson and L. H. Toburen: Energy and angular distributions of electrons from fast $He^+ + He$ collisions. *Phys. Rev. Lett.* **46**: 529–532; 1981.
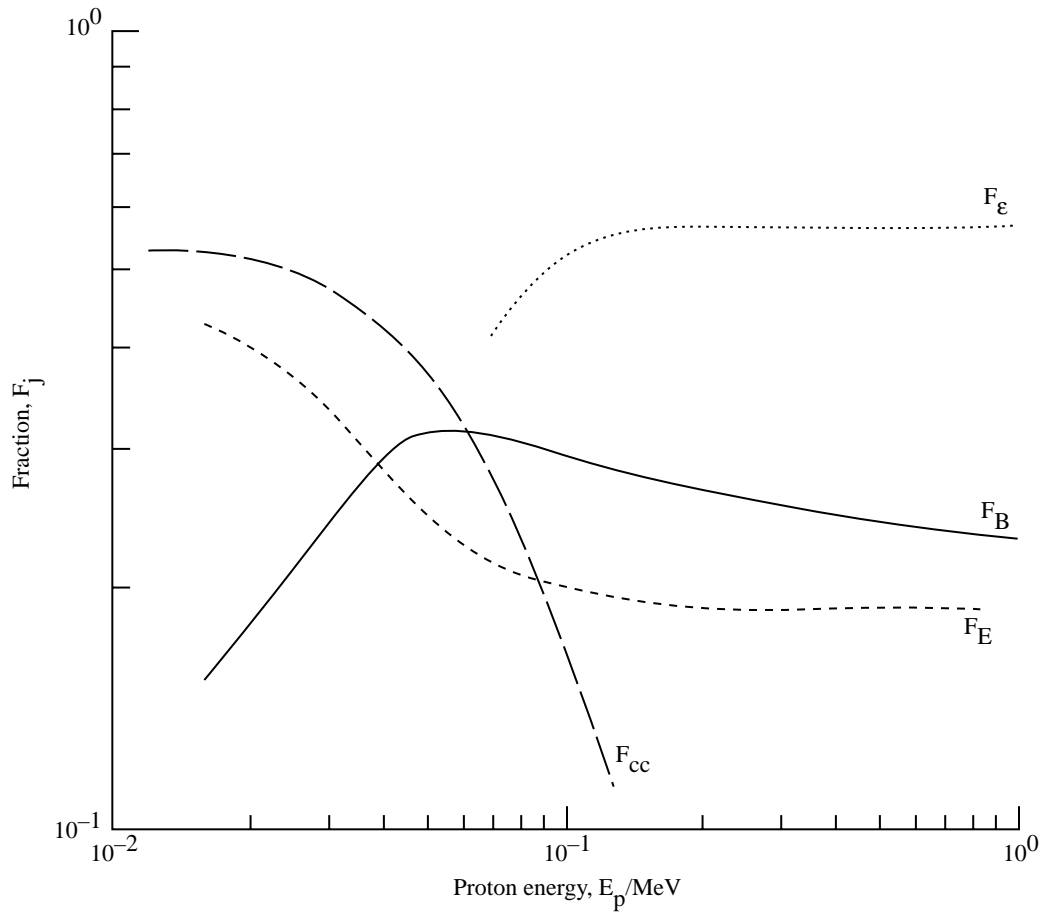
Figure 1.   Graph showing the fractions of the stopping power for protons incident on water vapor due to various processes: F_E excitation; F_{cc} charge transfer; F_B, overcoming binding energy of electrons; F_ε, kinetic energy given to ejected secondary electrons. The total fraction due to ionization is the sum $F_\varepsilon + F_B$. (Taken from Wilson, 1972.)
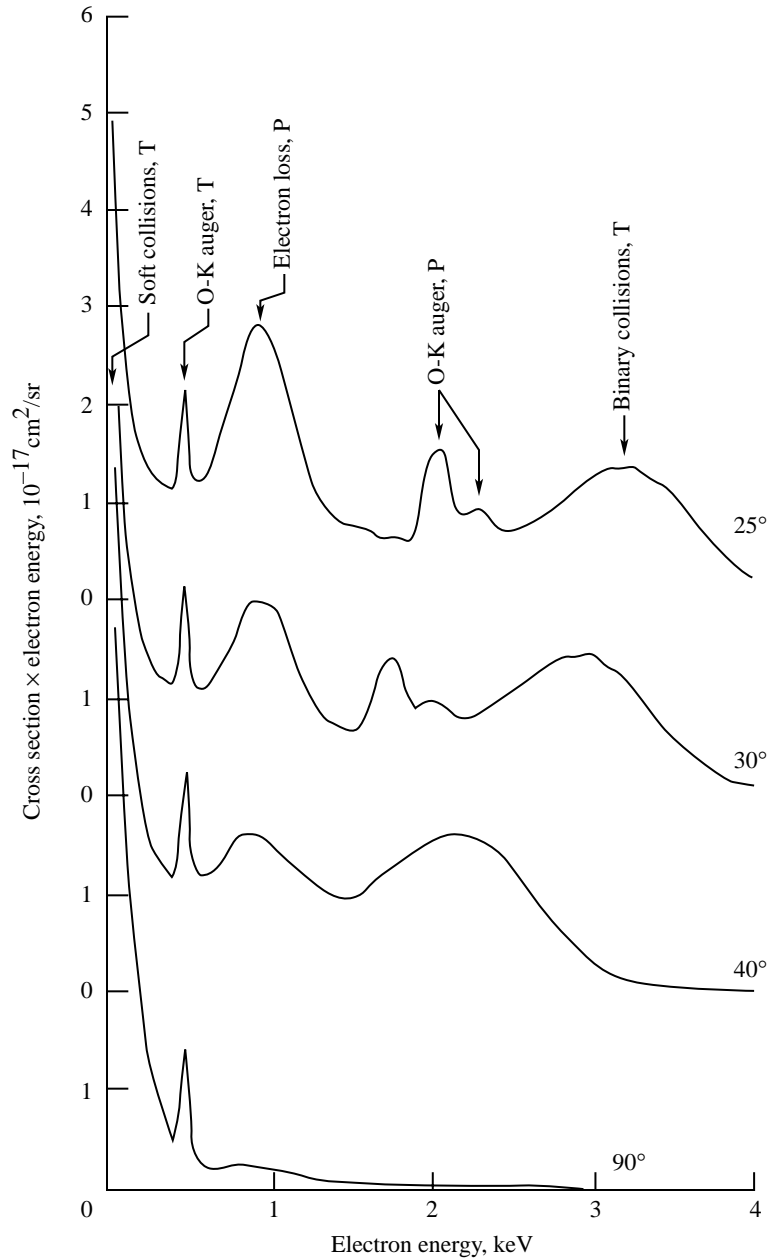
Figure 2. Energy spectra of electrons ejected at various angles from 30-MeV O^{5+} + O_2 collisions. *T* stands for emission from the target, *P* from the projectile. The binary collision peak comes at different energies for different angles. The Auger peak from the projectile also shifts with energy because of the kinematic effect of the moving source. (Taken from Stolterfoht, et al., 1974.)
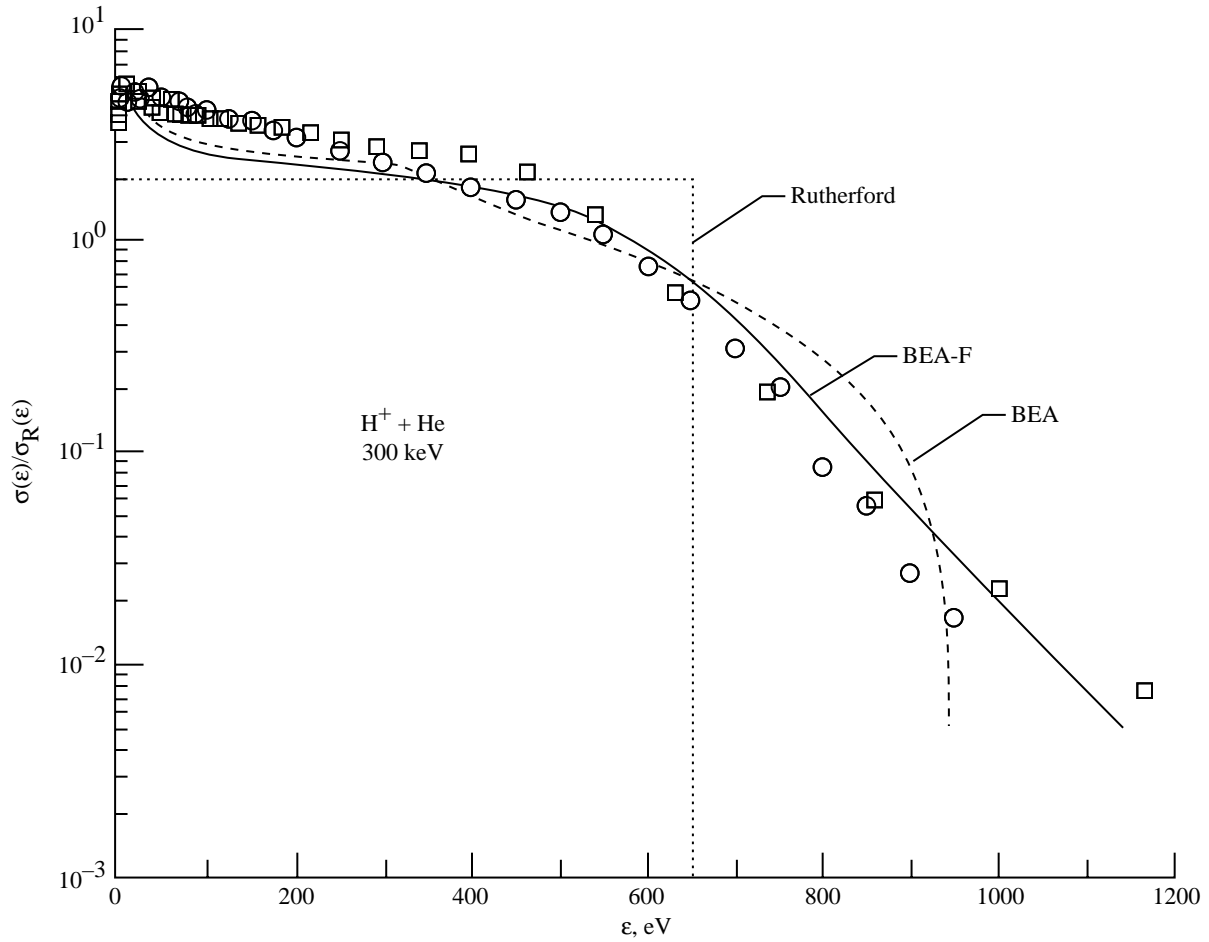
Figure 3.   Comparison of the Rutherford, the BEA, and the BEA-F equations with experiment for the energy spectrum of electrons from 300-keV H^+ + He collisions.
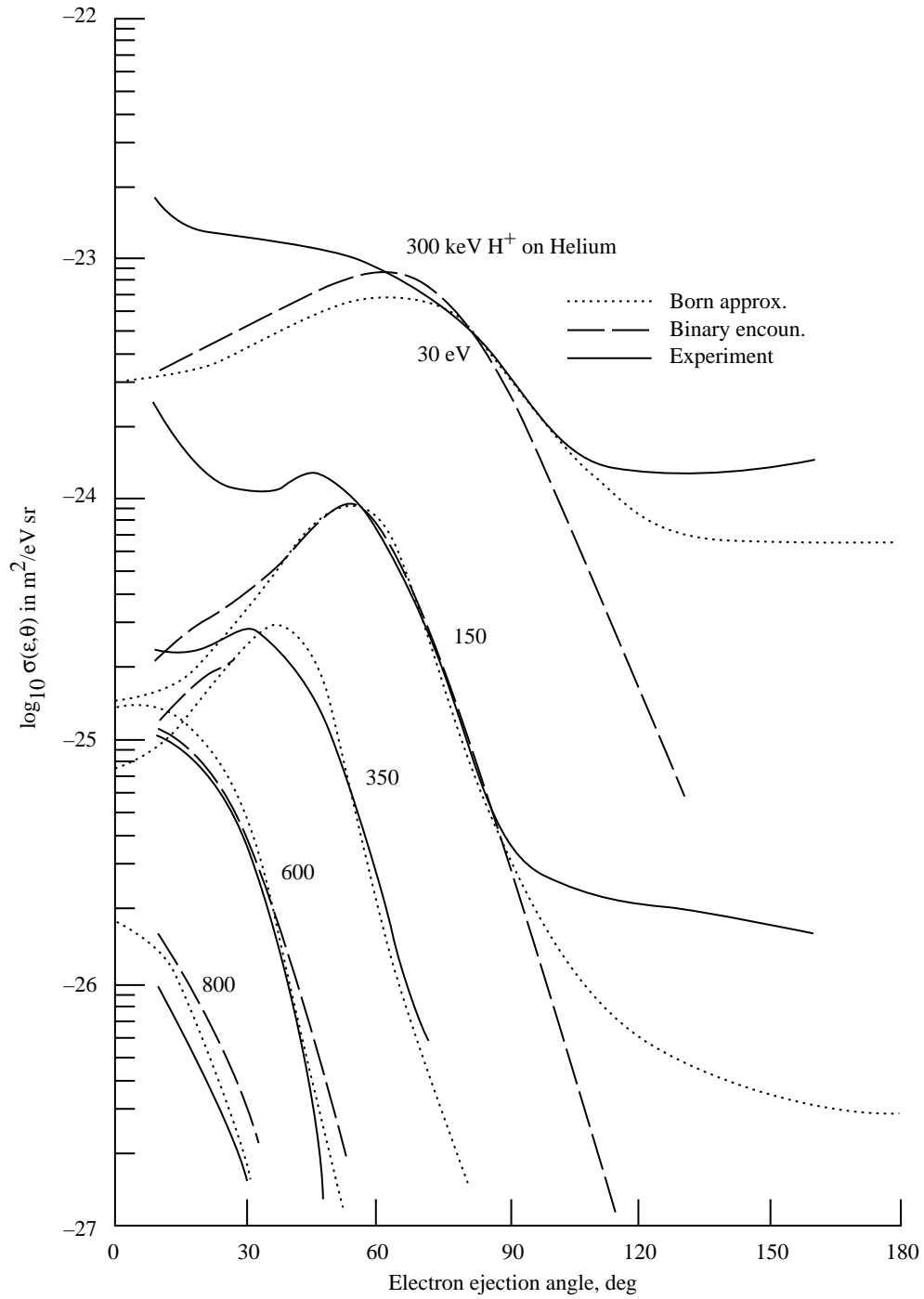
Figure 4. Comparison of the Born approximation and the BEA with experiment for angular distributions of electrons of 30 to 800 eV from 300-keV H$^+$ + He collisions. (Taken from Rudd and Macek, 1972.)
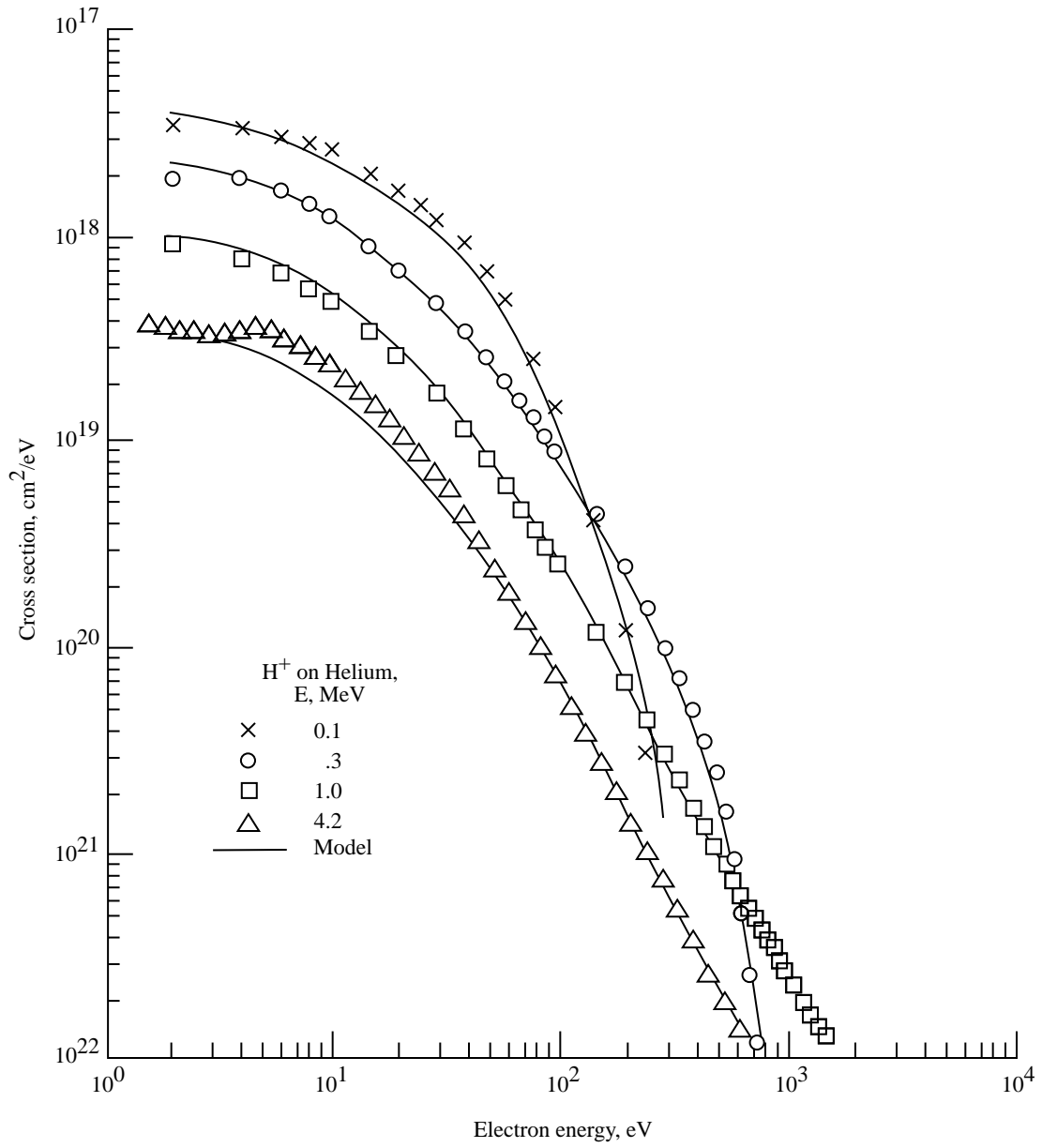
Figure 5.   Comparison of energy spectra calculated using the Miller model with experiment for four energies of protons on helium. (Taken from Miller et al., 1983.)
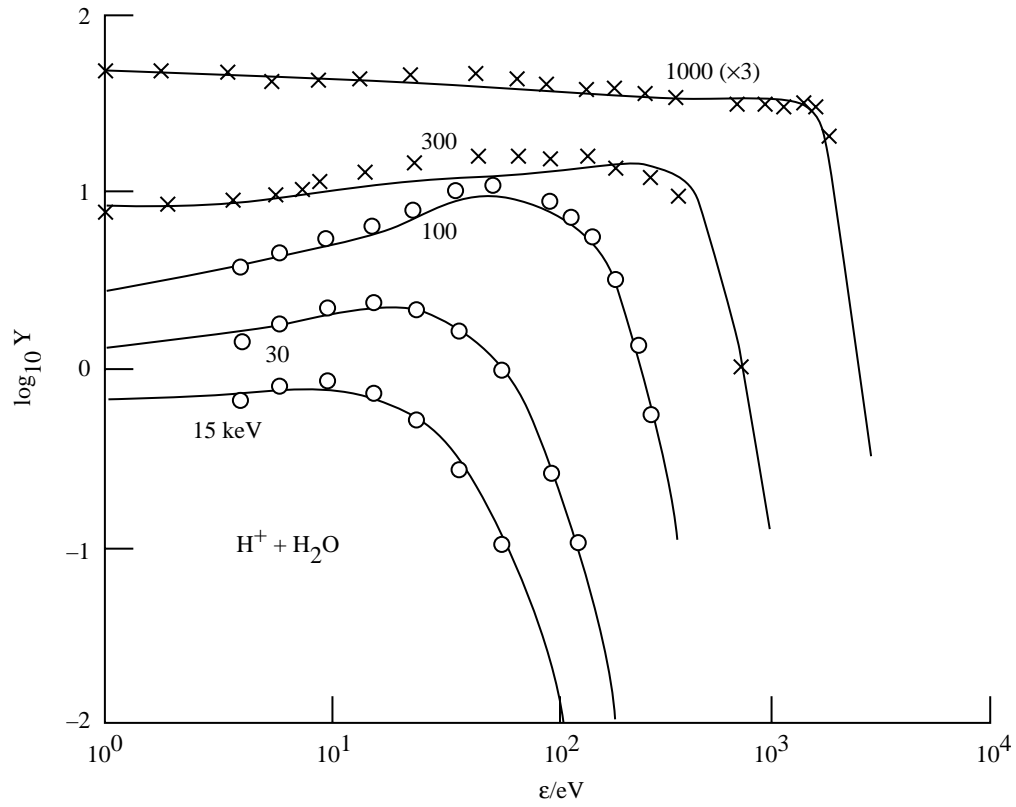
Figure 6. Comparison of the Rudd model with experimental values of cross sections for 15 keV to 1 MeV $H^+ + H_2O$ collisions. (Taken from Rudd et al., 1992.)
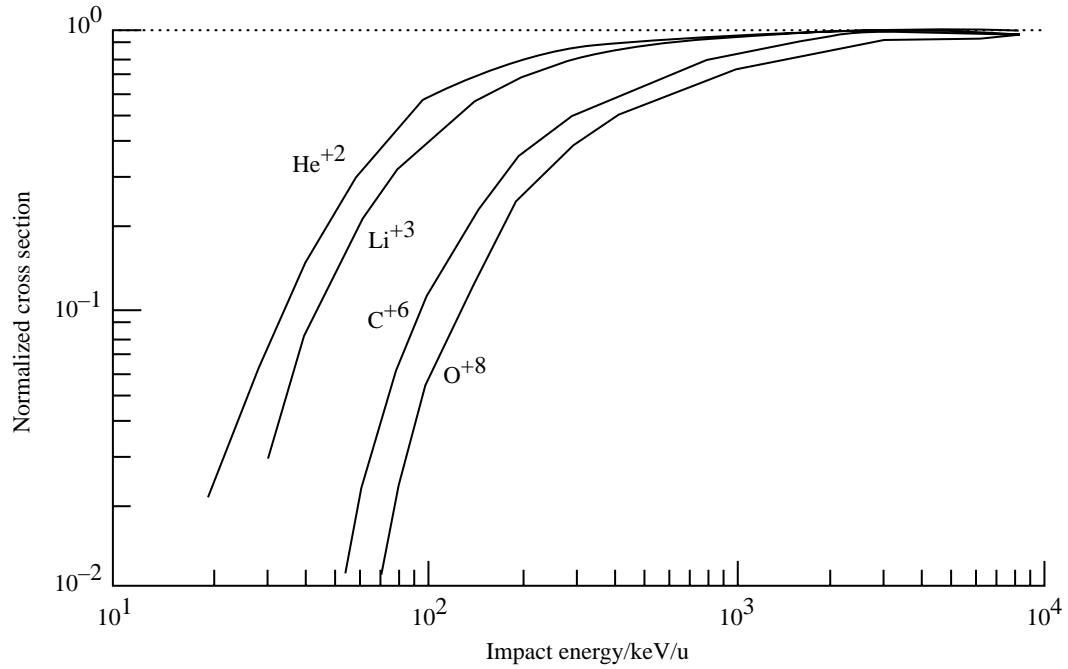
Figure 7.   The total ionization cross sections (TICSs) vs. impact energy per unit projectile mass. The TICSs have been normalized by dividing by Z^2 times the corresponding proton cross sections. The dotted line indicates expected results if Z^2 scaling held. (Taken from Fainstein, 1991.)
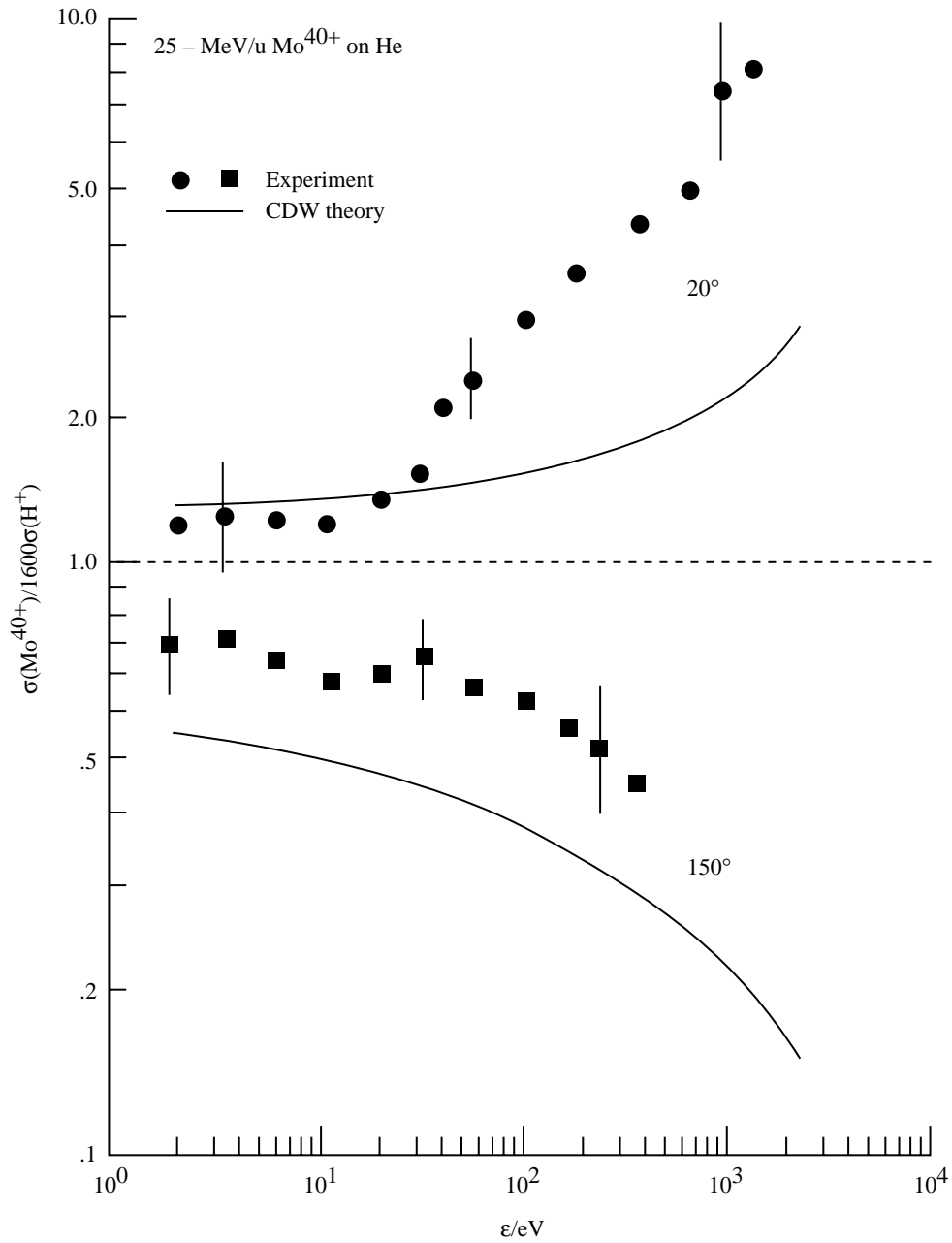
Figure 8.   Energy spectra of electrons at two emission angles for 25-MeV/u Mo^{40+} + He collisions. The cross sections have been normalized by dividing by 1600 times the equal-velocity proton values. The dashed line indicates the expected result if Z^2 scaling held. The solid line gives calculations using the CDW-EIS theory (see text). (Taken from Stolterfoht et al., 1987.)
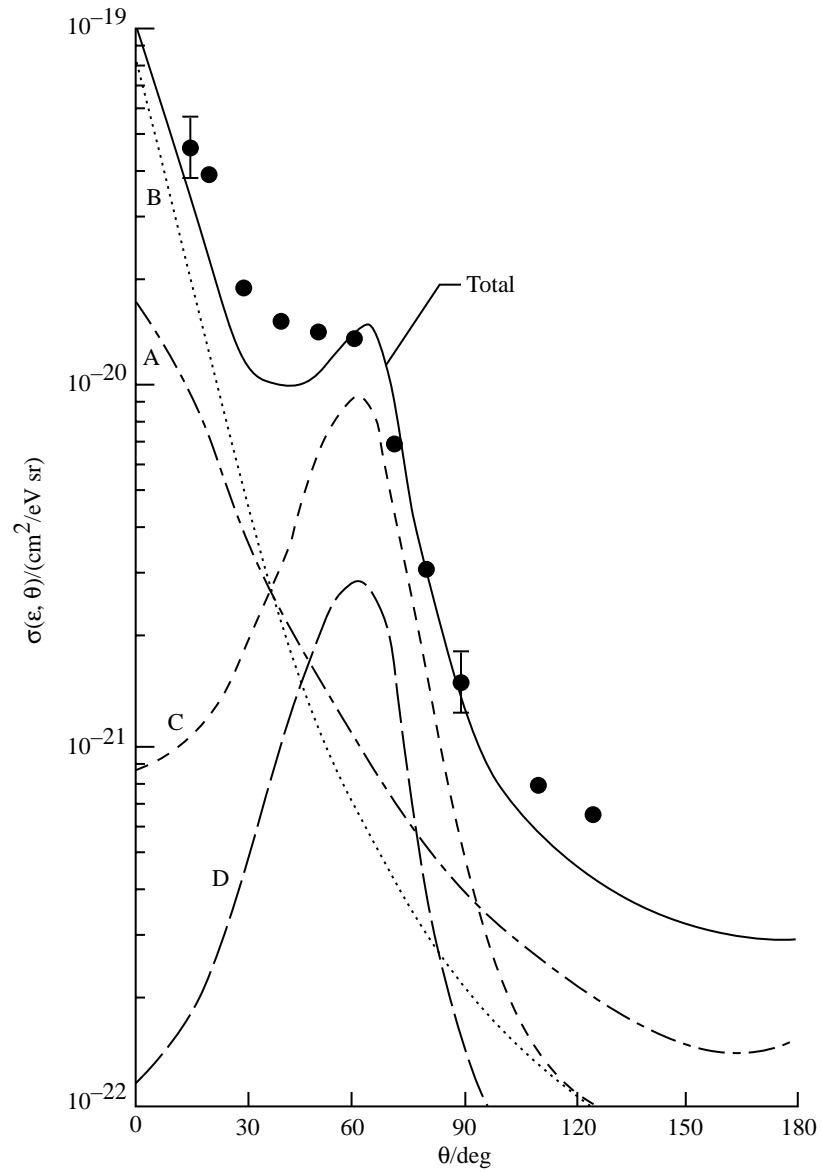
Figure 9.   Angular distribution of 218-eV electrons from 0.5 MeV/u He$^+$ + He collisions. Calculated values of four processes (see text) are added to give the total which is in fairly good agreement with experiment. (Taken from Manson and Toburen, 1981.)
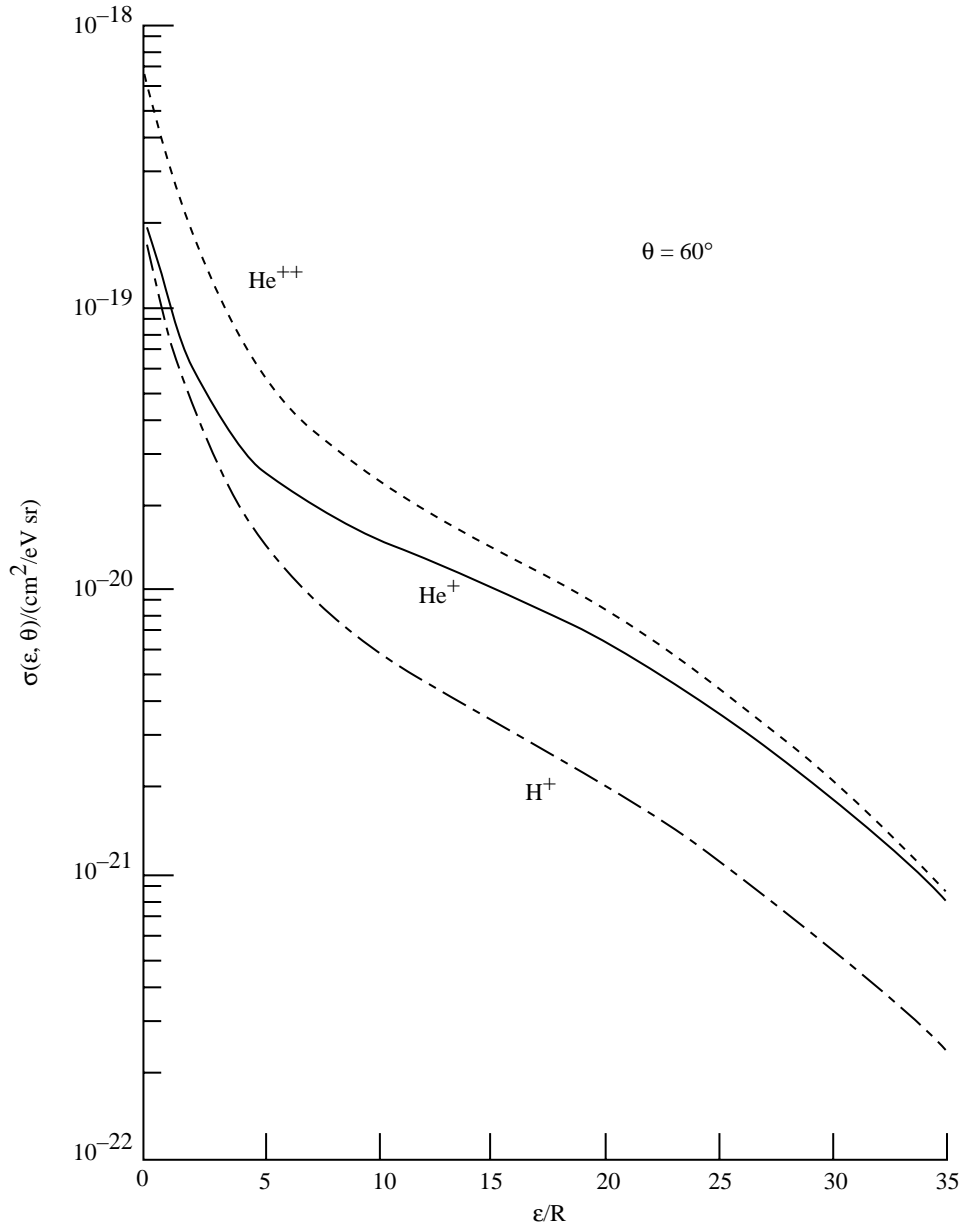
Figure 10. Energy spectra of electrons ejected at 60° from H^+, He^+, and He^{2+} collisions with helium to show how screening of the He^+ varies with ejection energy. (Taken from Manson and Toburen, 1981 [14].)